Development of Jurkat lymphocytes as a model to study the role of Zn^{2+} in T-cell immune function

Hannah McMullen
Department of Molecular Cellular and Developmental Biology
University of Colorado at Boulder
Spring 2017

Defense Date: April 7, 2017

Thesis Advisor:
Dr. Amy Palmer, Ph.D. (Department of Chemistry and Biochemistry)

Committee Members:
Dr. Jennifer Martin, Ph.D. (Department of Molecular Cellular and Developmental Biology)
Dr. Nancy Guild, Ph.D. (Department of Molecular Cellular and Developmental Biology)
Dr. Jennifer Knight, Ph.D. (Department of Molecular Cellular and Developmental Biology)

Table of Contents

I. Abstract

Zn^{2+} is an essential micronutrient, and the effect of Zn^{2+} deficiency is particularly evident in the diminished functioning of the immune system. There is growing evidence of Zn^{2+}'s involvement in immune function and its potential as a signaling species. Although the current literature supports importance of Zn^{2+} in the function of all immune cell types, we chose to focus our study on T cells particularly because of their role in orchestrating continued adaptive immune response. FRET based Zn^{2+} sensors have been used to reliably visualize Zn^{2+} in adherent cell types. We sought to develop a model system using Jurkat lymphocytes to apply these tools to parse out role of Zn^{2+} in T cell behavior. Over the course of the study, we optimized methods to transfect these tools into Jurkats, perform imaging, and ensure sensors were functioning properly. Additionally, we confirmed stimulation of the Jurkat cells to ensure proper T cell activation. We find that T cells have more free zinc than adherent cells, and that we can successfully stimulate them. With these tools in hand we hope to provide insight into Zn^{2+}'s role in T cell function.

II. Introduction:

a. Zn^{2+} biology in the immune system

Zn^{2+} is essential for human growth and proper function of every bodily system. Most notably, Zn^{2+} is necessary for growth, cognitive development, gastrointestinal function, and the ability to generate a robust immune system response.[1] Billions of people throughout the world suffer from Zn^{2+} deficiency, and because of Zn^{2+}'s involvement in so many different processes, the symptoms vary widely depending on the severity of the deficiency.[2,3] These include cognitive deficits, appetite disturbances and weight loss, underdevelopment, and increased susceptibility to bacterial and viral infections.[2] Of particular interest is the marked decrease in immune function that is observed under conditions of Zn^{2+} deficiency, raising the question of the nature of Zn^{2+}'s involvement in the mechanisms of immunity.[2]

The immune system is the body's system of defense against invading pathogens, including viruses, bacteria, and fungi, to prevent infection and illness.[4] The defense against these pathogens involves dozens of different cell types, each with highly specialized functions. When a pathogen gains access to the body, these cells work together to recognize the invading pathogen and mount a response to counteract it.[4] Immunity is divided into the categories of innate and adaptive immunity. These two categories involve different cell types that differ in the manner of recognition and response. Zn^{2+} has roles in both innate and adaptive immunity.[2–4]

Innate immunity functions constantly and nonspecifically against potential pathogens, through the use of soluble extracellular proteins and immune cells such as macrophages, natural killer cells, and neutrophils.[4] These cells do not have to recognize

the identity of the pathogen; they simply discern the invader as "non-self" and destroy them.[4] Zn^{2+} deficiency decreases the phagocytic activity of these cells, impairing the process by which they destroy pathogens.[2] This shows that Zn^{2+} is important for the functioning of the innate immune system, the body's first defense against an invading pathogen. When the immune system is functioning normally, the cells of innate immunity facilitate the activation of the cells of adaptive immunity if the mechanisms of innate immunity are inadequate to eliminate the pathogen.[4,5]

Adaptive immunity tunes the response of the immune system in a highly specific way towards the particular invading pathogen, using B cells and T cells to target the response.[4,5] B cells are responsible for producing antibodies, soluble proteins that recognize, bind, and facilitate the destruction of the specific pathogen.[5] T cells are divided into two subsets: CD8 or killer T cells, and CD4 or helper T cells. CD8 T cells are cytotoxic and kill virally infected cells. CD4 T cells, play an important role in the activation of many different immune cell types to maintain the immune response and are especially important for bacterial infection.[4,5] In the case of infection, T cells find their specific antigen presented on a major histocompatibility complex (MHC) molecule on a specialized antigen presenting cell, which can be a dendritic cell, macrophage, or B cell.[4,5] The T cell's T cell receptor (TCR) binds the MHC:antigen complex as the primary stimulatory signal (Figure 1, panel A).[5] A costimulatory signal between the T cell's CD28 molecule and the antigen presenting cell's B7 molecule is also required for activation; without this costimulatory signal, an inactivated state of anergy is induced and the T cell is unable to be activated (Fig 1, panel B).[5] Upon activation by the TCR and the costimulatory signal, an intracellular signaling cascade is initiated, resulting in activation

of the key transcription factors NFkB and NFAT.[5] These transcription factors translocate to the nucleus, where they initiate transcription of IL-2, which is a cytokine produced and secreted by the activated T cell (Figure 1, panel C).[5] Both B and T cells are unable to function properly under conditions of Zn^{2+} deficiency; B cells undergo apoptosis while T cells display overall decreased function, including decreased proliferation and decreased production of cytokines.[2]

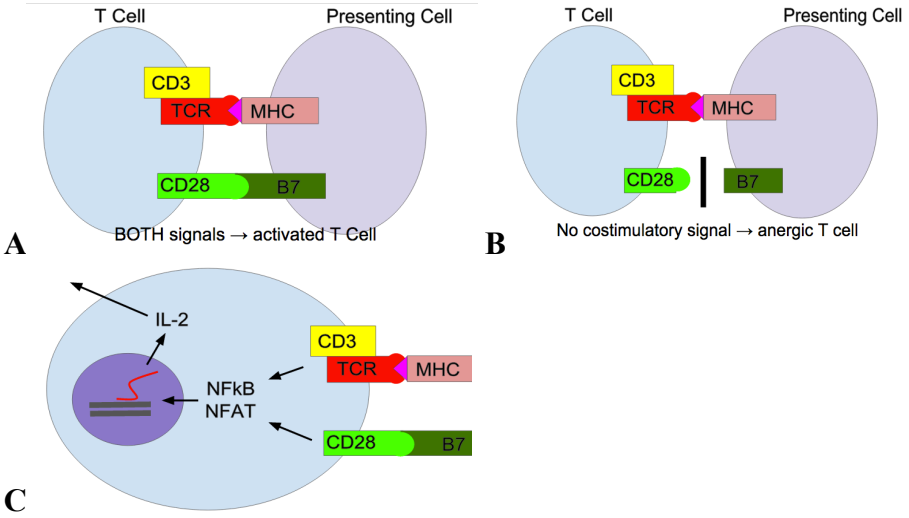

Figure 1: Native stimulatory interaction for T cell activation.
Panel A. Diagram of successful T cell activation through the recognition of MHC bound to antigen on an antigen presenting cell (APC) with the T cell receptor (TCR) and costimulatory signal of CD28 binding B7 on the APC. Panel B. Diagram of lack of costimulatory signal leading to state of T cell anergy. Panel C. Diagram of successful T cell activation leading to activation of transcription factors NFkB and NFAT and subsequent production and secretion of IL-2.

Because T cells orchestrate the response of other immune cell types, we chose to study the effect of Zn^{2+} on T cells as a key to understanding the role of Zn^{2+} in immune function. A few studies have been performed to assess the role of Zn^{2+} in T cell activation. T cells carry out this activation upon stimulation and release cytokines to

signal further activation of T cells and other immune cell types. IL-2 is a key cytokine released by T cells that acts in an autocrine and paracrine fashion, serving to drive the continued activation and proliferation of T cells (Figure 1, Panel C).[5] The role of Zn^{2+} in the intracellular pathways of T cell activation and IL-2 production has been explored by Kaltenberg et al, who found changes in cytosolic Zn^{2+} concentration altered the activation of key transcription factors for IL-2 production in murine cytotoxic T cells and primary human T cells.[6] One of the main proteins in the IL-2 receptor intracellular signaling pathway is ERK, which is an active kinase when phosphorylated and can be inactivated by phosphatases.[6] The active form of ERK is needed for T cell proliferation from IL-2 stimulation. Kaltenberg et al showed that ERK signaling is Zn^{2+} dependent by showing phosphorylation of ERK only under conditions where Zn^{2+} was present, and dephosphorylation of ERK under conditions of no Zn^{2+}.[6] This study suggests a role for Zn^{2+} signaling in T cell activation.

b. Current understanding of labile Zn^{2+} cell biology

Despite our understanding of the universal importance of Zn^{2+} at an organismal level, our knowledge of the roles of Zn^{2+} within the cell remains largely incomplete. A main goal of this study was to begin to apply what has been uncovered by Zn^{2+} biologist to clarify suggestions that have been made in the study of T cells. Most Zn^{2+} within the cell is protein-bound. It serves as a cofactor for many proteins in either a structural role by helping the protein assume its functional structure, or in a catalytic role as a key cofactor of enzyme active sites.[7] Although most intracellular Zn^{2+} is protein bound, there is growing interest about the small amount of free or labile Zn^{2+} in the cytosol.[8] The role of

this labile Zn^{2+} pool remains somewhat of a mystery, but holds the potential for a role as a signaling species within the cell.[9] The importance of Zn^{2+} is emphasized by its ubiquity and its extremely tight regulation within the cell by 24 transport proteins that move Zn^{2+} across membranes and 14 metallothioneins (MTs) that sequester excess Zn^{2+} in the cytosol.[10] Zn^{2+} transporters are divided into two main families that mobilize Zn^{2+} in opposing directions: ZIP transporters import Zn^{2+} into the cytoplasm, and ZnT transporters that export Zn^{2+} out of the cytoplasm.[7] Metallothioneins (MTs) are small, cysteine-rich peptides that bind Zn^{2+} in the cytosol and within certain organelles and regulate the local concentration of Zn^{2+}.[11] Both transport proteins and metallothioneins form a system of highly redundant proteins regulating Zn^{2+} within the cell. The system of Zn^{2+} homeostasis ensures that adequate Zn^{2+} is present for proper cell functioning while preventing accumulation of excess intracellular Zn^{2+}. This is important because although essential in trace amounts, a large amount of Zn^{2+} is toxic to cells.[12]

Main questions that Zn^{2+} biologists seek to address are: What cell processes require Zn^{2+}, and how can perturbation of Zn^{2+} homeostasis impact these processes? Which proteins sense and respond to environmental Zn^{2+} to maintain Zn^{2+} homeostasis throughout different cellular functions including proliferation, stimulation, and apoptosis? Does the perturbation of these homeostasis proteins affect cellular function? Investigating the system of proteins involved in Zn^{2+} homeostasis presents the opportunity to identify the role of Zn^{2+} in orchestrating, initiating, or maintaining healthy cellular responses.

For disturbances in Zn^{2+} to be meaningful to cells and impact cell processes, the cells must be able to detect the disturbance. Proteins that regulate the transcription of multiple genes involved in Zn^{2+} homeostasis are of particular interest because of their

increased potential to alter Zn^{2+} regulation within the cell by detecting disturbances in Zn^{2+}. One such potential sensor is metal regulatory transcription factor 1 (MTF1), a nucleocytoplasmic shuttling protein.[13] In the presence of heavy metals such as cadmium, Zn^{2+}, copper, and silver, MTF1 re-localizes to the nucleus. In the nucleus, MTF1 binds to promoters with a metal-responsive element (MRE) to induce expression of proteins that regulate the amount of metal within the cell such as metallothioneins and other metal homeostasis genes.[13] Hardyman et al have shown previously that MTF1 knockdown causes expression changes of several Zn^{2+} -regulating proteins in response to increased Zn^{2+}, including SLC30A1 (ZnT1), MT1F, MT1B, MT2A, MT1M, MT1E, MT1G, and MT1H.[13] Hardyman and co-workers knocked down expression of MTF1 and found that these proteins no longer display altered expression in response to excess Zn^{2+}.[13] These results suggest that without MTF1, the expression of these proteins is no longer sensitive or responsive to Zn^{2+}. These proteins are all involved in limiting the accumulation of excess Zn^{2+} within the cell, such as SLC30A1 which downregulates Zn^{2+} influx.[13] Given the importance of Zn^{2+} in the function of T cells, this raises the question of the importance of Zn^{2+} -sensing proteins such as MTF1 in the proper activation of T cells. Are T cells able to maintain Zn^{2+} homeostasis and be successfully activated without MTF1?

c. Zn^{2+} sensors

Zn^{2+} sensors allow us to visualize labile Zn^{2+} within the cell, providing new insights into Zn^{2+} biology. Zn^{2+} sensors have been developed in two major classes: small molecule probes and genetically encoded sensors[14,15]. In contrast to small molecule probes which are designed to be cell permeable and concentrate acutely in cells, our

sensors are genetically encoded and expressed in cells either transiently for days or stably integrated into the genome of a cell type.[15] A benefit of our genetically encoded sensors is that they are constitutively expressed by the cell at 1-10uM; this is a low enough concentration that the sensors don't significantly impact the buffering of Zn^{2+} themselves[14]. Genetically encoded sensors can be either FRET based or intensity based. FRET based sensors have the added benefit that they are ratiometric, and therefore the signal can be normalized to account for possible heterogeneity in samples, including cell thickness and sensor concentration.[15] For our FRET sensors, when Zn^{2+} binds, the conformation of the sensor changes to bring the two fluorescent proteins (FPs) into a more favorable orientation for energy transfer between the FPs than when they are in the Zn^{2+} unbound state, resulting in an increase in the FRET ratio (R) (Figure 2).[14–16] We define the FRET ratio as the intensity of the energy emitted from the FP that accepts the transferred energy over the emission intensity from the excited donor FP (see Equation 1).[15] Zn^{2+} concentration can be calculated by measuring the saturation of the sensor and the affinity of the sensor for Zn^{2+} . The fractional saturation of the sensor is determined by a calibration measuring the sensor signal in the resting, apo, and Zn^{2+} -bound states (Figure 2).[15] Measurement of the sensor in the free and unbound or apo state is induced by introducing sufficient amounts of a chelating agent, N,N,N',N'-Tetrakis(2-pyridylmethyl)ethylenediamine (TPEN) or tris(2-pyridylmethyl)amine (TPA), to bind the intracellular Zn^{2+}, seen in Figure 2 as R_{apo}.[15] The bound state signal is measured by introducing saturating amounts of Zn^{2+} along with agents to permeabilize the cell to deliver the Zn^{2+} intracellularly, or $RZn^{2+}{}_{bound}$ in Figure 2.[15] The fractional saturation is the percentage of sensor that is Zn^{2+} -bound in the resting state of the cell.

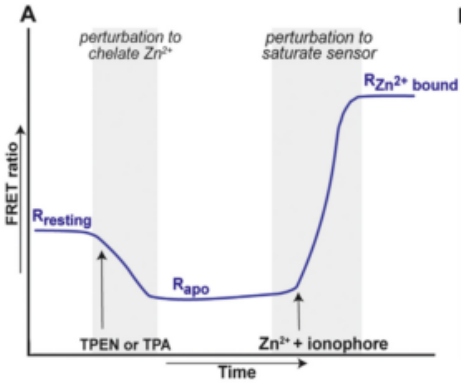

Figure 2: Diagram of FRET sensor calibration.
Figure adapted from Ref 15

Equation 1:

$$\boldsymbol{FRET\ Ratio = \frac{acceptor\ FP\ FRET}{donor\ FP\ emission}}$$

Our Zn^{2+} sensors are built with several useful design considerations. They are modular, with segments flanked by restriction sites to allow switching of the modules, allowing the sensors to be improved or optimized for particular applications via different approaches (Figure 3).[15] The main modules of a sensor are a targeting sequence that localize the sensor within the cell, two fluorescent proteins (FPs), the Zn^{2+} binding domain (ZBD): two Zn^{2+} fingers of Zap, a Zn^{2+} sensing protein from yeast, and the linkers that connect each FP to an end of the ZBD.[15] Targeting sequences can be altered in order to direct the sensor to an organelle or subcellular location. For example, a nuclear exclusion sequence (NES) can be attached to a sensor to exclude it from the nucleus and produce cytosolic localization. In contrast, a nuclear localization sequence (NLS) will direct the sensor to the nucleus of the cell.[17] Different signal sequences will result in selective targeting of the sensor to an organelle of the cell, allowing the local

concentration of Zn^{2+} to be measured within subcellular compartments.[15] Different FPs can be used per the photophysical requirements of a project. Since our lab uses yellow/blue sensors, FPs in other colors such as red can be used to tag other particles or components of interest or to mark expression of another tool such as shRNA at the same time. The sensor used in this study, ZapCV2 uses a cyan FP (CFP) as the donor, and an improved yellow FP (Venus) as the acceptor.[18] An important aspect of the sensors is their dynamic range, which is defined as the FRET ratio in the bound sate over the FRET ratio in the unbound state.[15] High dynamic range decreases the noise in sensor response and allows for accurate determination of the fractional saturation of a sensor. The dynamic range of ZapCV2 was optimized in the cytosol using circularly permuted Venus as the acceptor FP. Using this FP changes the overall orientation of the two FPs in relation to each other, changing the efficiency of energy transfer. Because of its high dynamic range ZapCV2 allows for accurate determination of Zn^{2+} concentration and can be used to monitor changes of Zn^{2+} concentration in the cytosol. The affinity of the Zn^{2+} sensors can also be optimized to the application of interest. If the affinity for Zn^{2+} is too high, the sensor will be fully saturated at a lower concentration of Zn^{2+} and be unable to reflect the true local concentration that is present if it is over that threshold. Zap2 is the Zn^{2+} binding domain of ZapCV2, and it has been mutated with a single amino acid substitution of a cysteine to a histidine to lower the affinity of the sensor for Zn^{2+} (Figure 4). The sensor is partially saturated in the cytosol under most conditions allowing for the detection of changes of cytosolic Zn^{2+}.

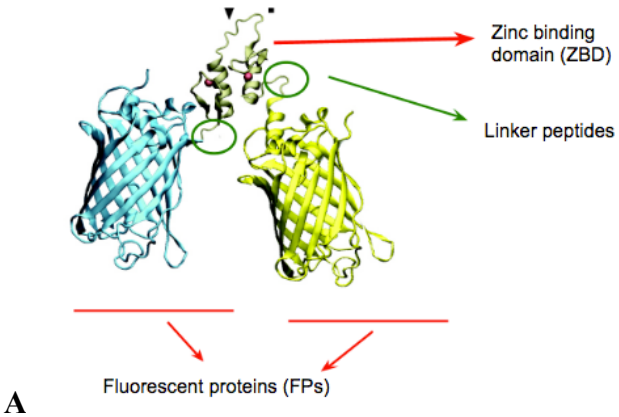

A

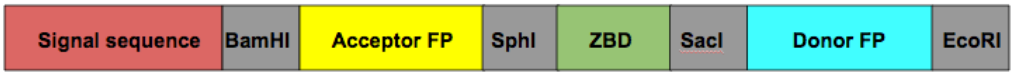

B

Figure 3: The modularity of ZapCV2.
Panel A. Diagram of the protein structure of the sensor showing the two FP's linked to the ZBD. Panel B. Schematic of the cloning of the sensors. Each major component is separated by a restriction site (highlighted in gray) allowing for easy interchange of components.

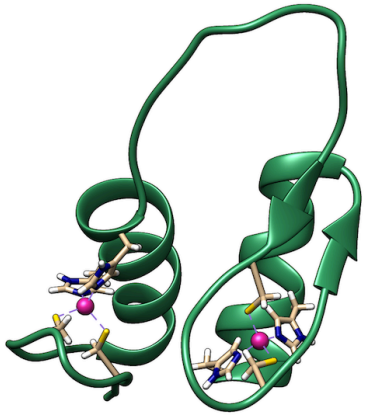

Figure 4: Crystal structure of the native Zap1 domain
(Zn^{2+} shown in pink) with coordinating amino acids highlighted. In ZapCV2 a Cys residue in each binding site has been mutated to a His to lower the affinity of the sensor. PBD entry 1ZW8.

Prior to my study, these sensors had been applied only to adherent cell lines to define the concentration of Zn^{2+} in the cytosol. The goals of the application of this tool were two-fold. The first goal was to define the concentration of labile Zn^{2+} in the cytosol of immune cells, which had not been done before. The second goal was to see if perturbations either to MTF1 (a Zn^{2+} sensing protein), the Zn^{2+} growth conditions, or the activation state of the cells altered the cytosolic Zn^{2+} concentration.

d. Jurkat cells as a model system

Given the importance of Zn^{2+} in the immune system, it became of interest to investigate Zn^{2+} in T cells with the FRET sensors developed by our lab. Jurkat cells are a human T cell lymphoblast line that grow in suspension in cell culture.[19] These were selected for the work in this thesis because of their ability to be stimulated by antibodies in vitro, well-documented potential for IL-2 production, their ability to be transfected, and because they are easier to obtain and manipulate than primary human T cells.[19]

III. Main Goals

The primary aim of the work in this thesis was to apply zinc sensors as a tool to effectively study the zinc biology within T cells, using Jurkat cells as a model. It became necessary as another aim to troubleshoot protocols in order to successfully work with the Jurkat cells, a novel cell type in the lab. There were two primary areas that we chose to investigate.

First, we wanted to see if we could perturb proteins involved in Zn^{2+} homeostasis and observe a change in intracellular Zn^{2+} concentration. In order to investigate this question, we selected MTF1 as the zinc homeostasis protein of interest, knocked down its expression through transfection with shRNA, and monitored cytosolic zinc concentration with the NES-ZapCV2 sensor. Since MTF1 plays a role in the expression of many different zinc transporters and metallothioneins, we hypothesized that knocking down MTF1 could diminish the cells' ability to detect and respond to a disturbance in zinc concentration. We hypothesized that this could lead to an inability to export excess zinc from the cytosol and lead to a higher concentration of cytosolic zinc.

Second, we wanted to investigate the role of Zn^{2+} in T cell stimulation with the Jurkats as the model T cells. Zn^{2+} is highly important for T cell stimulation, activation, and effector functions. We wanted to first confirm the results shown by Kaltenberg and colleagues that show an increase in cytosolic Zn^{2+} concentration upon stimulation. By using our Zn^{2+} sensors rather than small molecule probes, the cytosolic Zn^{2+} concentration could be more accurately calculated. We also wanted to investigate the other side of the story and see if stimulation of the T cell is impacted by differences in the Zn^{2+} availability in the local environment of the cell. This is of particular interest when considering the detrimental effects on the immune

system of Zn^{2+} deficiency, and could support diminished T cell activation as playing a role in the decreased ability of the immune system to function in conditions of low Zn^{2+}. Additionally, it is of interest to see whether T cell stimulation is affected by conditions of relatively high Zn^{2+}.

IV. Methods

a. HeLa cell culture

HeLa cells were used as a first model mammalian cell line in order to learn about working with cells in cell culture and imaging techniques prior to working with Jurkat cells. HeLa cells were split or passaged at least every 5 days to maintain optimum growing density and cell health. First, all media was suctioned off with an aspirating pipette. The plate was then washed with 10 mL of phosphate-buffered saline (PBS). Cells were incubated at 37°C for 2-3 minutes with 2.5 mL of warmed trypsin to degrade adhesion proteins and free cells from the plate. 7.5 mL of warmed Dulbecco's Modified Eagle Medium (DMEM) with Fetal Bovine Serum (FBS) was added. A fifth of the resulting cell suspension was then added to a fresh 10 cm dish, and new DMEM was added to achieve a total volume of 10 mL. Plates were returned to the incubator for storage at 37°C and 5% CO_2.

b. Jurkat cell culture

Jurkat E6-1 cells were acquired from ATCC (American Type Culture Collection) and were grown in RPMI-1640 medium supplemented with 10% FBS. Jurkat cells require special consideration for cell culture protocols because they are suspension cells, and so cannot be split in the same manner as the adherent HeLa cells. Jurkat cells have a doubling time of 48 hrs. The cells were split approximately every 3 days in a 1:5 ratio or 1:10 ratio as the cell density required.

After thawing, blasticidin treatment, or to maintain health of cells, the following additional steps were taken to ensure cell health. These steps were performed when cultures contained a considerable number of dead cells and debris. The cultures were

spun down at 500 rpm for 5 minutes to pellet live cells while leaving most debris in the supernatant. After spinning, the supernatant was removed, and cells were resuspended in fresh RPMI at a density of ~$1x10^5$ cells/mL.

c. Transfection of Jurkat cells

TransIt

The first method of transfection attempted was the lipid-based TransIt transfection regent and protocol developed by Mirus Bio LLC. The manufacturer's protocol was followed, using 125uL optimem, 0.5uL zap-CV2 DNA, 3uL TransIt, and $5x10^4$ cells/well.

Electroporation: Neon Transfection System

The Neon Transfection System was used to electroporate the Jurkat cells, which works by creating an electrical field that opens pores in the cells for the DNA to enter. The parameters recommended by the manufacturer for immune cells were used for this study: 1400V, 1 pulse, 30ms, 5 ug DNA, and $5x10^6$ cells.

d. Creation of stable NES-ZapCv2 Jurkat cell line

The PiggyBac Transposon Vector System was used to create a line of Jurkat cells stably expressing the NES-ZapCv2 sensor. The PiggyBac (PB) is a transposon that works with the transposase to insert a gene or segment of DNA into the genome of a host cell. In this study, it was used to insert the DNA for the NES-ZapCv2 sensor into the genome of the Jurkat cells.

Blasticidin kill curve

The PiggyBac system that was used contains in its vector a gene conferring resistance to the antibiotic blasticidin. In order to use blasticidin to select for cells that

successfully received the gene of interest, a blasticidin kill curve of Jurkat cells was constructed. This was done by plating Jurkat cells with different concentrations of blasticidin (20, 15, 10, 5, 2.5, 1 ug/mL) to determine the concentration at which the cells die. The lowest concentration at which the cells were dead after two days of treatment was 15 ug/mL, so this concentration was used for selection of successfully transfected cells.

Transfection with ZapCv2 and transposase

A dual transfection was performed using the Neon Transfection System for electroporation according to the protocol described previously. Briefly, 5 ug ZapCV2 in the PiggyBac vector (to a concentration of 350ng/uL) and 10ug transposase DNA (to a concentration of 300ng/uL) were used to transduce $6x10^6$ cells. The electroporated Jurkat cells were then grown in 15 ug/mL blasticidin for 10 days. Successful transformation was further confirmed by the expression of the NES-ZapCV2 sensor in all cells.

Cryopreservation

The stable NES-ZapCv2 Jurkat cells were prepared in $1x10^5$ cell aliquots in RPMI media in 1.5mL cryopreservation tubes. DMSO (dimethyl sulfoxide) was added to a concentration of 5% to prevent ice crystal formation and cell damage. The tubes were stored in the -80C freezer for two days before storage in the -140°C liquid nitrogen cryofreezer.

e. Imaging

Sample preparation

The Jurkats were counted and plated before incubation. When cells were expressing sensor stably about half as many cells were needed for imaging. The Jurkats

were transfected with the Neon transfection system according to the parameters described above and incubated for 2 days at 37°C and 5% CO_2. The cells were pelleted in a 15 mL tube by spinning at 500rpm for 5 minutes. The supernatant media was removed by aspiration. This was followed by a wash step to remove residual media by adding 5mL of HHBSS Ca/Mg/phosphate- free imaging buffer. This imaging buffer is used because of its low background fluorescence and ability to maintain short term cell health, allowing for successful imaging of cells. The cells were pelleted again by another 500 rpm spin for 5 min. The cells were re-suspended in 2-4 mL of the imaging buffer with the amount depending on desired cell density, and plated on 35 mm poly-L-lysine (PLL)-coated imaging dishes. The imaging dishes were spun for 1 min at 800 rpm in the plate-spinning inserts of the centrifuge. Plate was placed in 37°C environmental chamber to warm for 15min before imaging.

Poly-L-Lysine (PLL) coated plates

PLL-coated plates were used to minimize cell movement and allow the cells to settle to the bottom of the imaging dish and spread out. 1mL of PLL solution at a concentration of 10 ng/mL was applied to each 35mm small imaging dish the day prior to imaging and stored in refrigerator overnight. Before use, the PLL solution was aspirated off and the plates were washed 3 times with milli-Q ultrapure water.

Poly-L-Lysine (PLL) was compared to Poly-D-Lysine (PDL) coated plates. To prepare PDL-coated plates, PDL stock at 10 ng/mL was diluted in milli-Q water and applied to imaging dishes at a final concentration of 1ng/mL. PDL plates were stored and washed according to the same protocol described for PLL plates prior to sample application, and no difference in reduction of cell movement was observed.

Calibration of Jurkat cells

Calibrations measure resting, maximum, and minimum values of Zn^{2+} sensor saturation. Such calibrations are typically performed by measuring resting sensor signal, adding a chelating agent and measuring the resulting minimum signal, washing out the chelating agent, and adding sufficient Zn^{2+} for saturation and measuring the resulting maximum signal. Since the Jurkats are suspension cells, this must be done differently than a classic calibration because the chelator TPA cannot be washed out without washing away the cells. Instead, the saturating solution: 1 uM Zn, 0.5 uM pyrithione, and 0.001% saponin, was added first to achieve maximum FRET ratio and saturate the sensor. Then, excess TPA (50 uM) was added to bind the Zn^{2+}, create apo-sensor, and achieve the minimum FRET ratio. The protocol for this calibration is described below.

Calibration Protocol

The samples were prepared for imaging as described above. After a 15 minute incubation in the environmental chamber on the microscope, each channel was measured every minute until a stable resting signal was recorded. Then, the prepared Zn^{2+} solution was added to achieve a final concentration of 1uM Zn^{2+}, 0.5uM pyrithione, and 0.001% saponin. Each channel was measured every 20 seconds for 3-5 minutes until a stable R_{max} signal was recorded. Then, the prepared TPA solution was added to achieve a final concentration of 50uM, and measurements were recorded every 20 seconds until a stable R_{min} signal was recorded.

Microscope Settings

The images were collected using the 40X oil objective lens of a Nikon fluorescence microscope. ND (Neutral Density) filters were used to alter the intensity of

light applied to the sample. Use of different ND filters allows adjustment depending on the brightness of the sensor to obtain visible images. The ND4 filter allows for 25% transmittance of light, and was used for imaging conducted on 11/6, 11/11, 12/8, and 1/13. The ND8 filter allows for 12.5% transmittance, and was used for imaging conducted on 10/28.

The following settings were used for all imaging (except where indicated) prior to 1/13/17:

Channel	Exposure	EM Gain	EM Gain Multiplier	Conversion Gain
YFP FRET	300ms	1 MHz, 16 bit	200,000	1X
YFP em	300ms	1 MHz, 16 bit	200,000	1X
CFP	300ms	1 MHz, 16 bit	200,000	1X
mCherry	200ms	1 MHz, 16 bit	200,000	1X

*Note: On 11/11 the mCherry gain multiplier was 300,000

After 1/13/17, the light was changed on the microscope, and the settings were as follows:

Channel	Exposure	EM Gain	EM Gain Multiplier	Conversion Gain
YFP FRET	300ms	1 MHz, 16 bit	300,000	1X
YFP em	300ms	1 MHz, 16 bit	300,000	1X
CFP	300ms	1 MHz, 16 bit	300,000	1X

Calculations of imaging data

The following equations were used to calculate the fractional saturation and dynamic range of the sensor ZapCV2. The average of the FRET ratios recorded at all

resting time points resulted in the "resting" variable. R_{max} was obtained by taking the average of the FRET ratios recorded at all time points after addition of the Zn^{2+} solution and before addition of TPA. R_{min} was obtained by taking the average of the FRET ratios at all time points after addition of TPA.

$$\boldsymbol{Fractional\ saturation} = \frac{(\boldsymbol{Resting - Rmin})}{(\boldsymbol{Rmax - Rmin})}$$

$$\boldsymbol{Dynamic\ range} = \frac{\boldsymbol{Rmax}}{\boldsymbol{Rmin}}$$

f. Zn^{2+} growth conditions

Proliferation assay

Wild type Jurkat cells were grown in different Zn^{2+} concentrations and cells were counted with a hemocytometer after 1 and 4 days. Counting with the hemocytometer was carried out after mixing 100 uL of cell solution with 100 uL of trypan blue to distinguish live cells from dead cells (which stain blue with trypan blue), and provide an accurate live cell count. Cells were originally plated at a density of $1x10^5$ cells/well. Zn^{2+} free media was made by adding Chelex resin to the FBS used to make RPMI, and supplementing back calcium that was lost as a result of chelation. The residual Zn^{2+} concentration in RPMI after Chelex treatment is about 2 uM as determined by inductively coupled plasma-mass spectrometry (ICP-MS). Zn^{2+} conditions were introduced by adding the appropriate amount of a filtered 1 mM $ZnCl_2$ stock that was prepared by a 10-fold dilution of a 1M $ZnCl_2$ stock. The 1 M $ZnCl_2$ stock was prepared by dissolving solid $ZnCl_2$ in milliQ H_2O.

When possible and when treated with Zn conditions, optimal cell health was obtained when cells were placed in the 37°C incubator on a constant rotator.

Imaging under different Zn conditions

First trial: Jurkats were grown in 0 uM (low condition), 20 uM (high proliferation condition, 80 uM (stressed condition) Zn^{2+} for 4 days before imaging. PLL coated plates were used, and a calibration was performed according to the protocol described previously.

Second trial: Jurkats were grown in 0 uM, 20 uM, 50 uM Zn^{2+} for 4 days before imaging. PDL coated plates were used, and a calibration was performed. Data was obtained for the 20 uM and 50 uM conditions only.

g. Stimulation of Jurkat cells

PMA/ionomycin

Jurkat cells were prepared in a 96 well plate in 200 uL of RPMI media. 200 ng/mL phorbol mysristate acetate (PMA) and 300 ng/mL ionomycin were added. Cells were observed with the wide-field microscope.

Anti- CD3/CD28 Antibody: Dynabeads stimulation

Dynabeads are coated with anti-CD3 and CD28 antibodies to bind and activate the T cells. This mimics the in vivo presentation of antigen-presenting cells and naïve T cells via cell surface receptors and subsequent activation of NFAT and NFkB to produce IL-2. IL-2 production was measured with an ELISA assay.

h. IL-2 ELISA (Enzyme-Linked Immunosorbent Assay)

A trial run of ELISA was performed to confirm stimulation with Dynabeads. Stable NES-ZapCv2 Jurkats were plated with $8x10^4$ cells in 200uL of RPMI media per

well. 2 uL of pre-washed Dynabeads were added to each well per manufacturer's instructions. Supernatant samples of 50 uL were pulled at the following time points: 0, 2, 4, 6, 22, 24, 96 hours. The samples were placed into pre-chilled Eppendorf tubes for storage and frozen in the -80°C freezer until the ELISA was performed. ELISA was prepared per manufacturer's instructions, including generation of a standard curve with IL-2.

The ELISA plate was imaged on the Tecan Safire II plate reader to measure absorbance of the samples at 450 nm. Absorbance intensity at 550 nm was used as an internal standard for probe concentration.

V. Results

a. Transfection techniques for Jurkat cells

In order to study Zn^{2+} in Jurkat cells, a protocol first had to be developed to introduce the DNA for the sensor into the cells. Working with suspension cells such as Jurkats was a new endeavor for the Palmer lab, so a new protocol to obtain high transfection efficiency was optimized. The first method of transfection attempted was the TransIt system, which is commonly used by Palmer lab members to successfully transfect adherent cells. However, in Jurkats the TransIt system resulted in a high death rate and ~10% transfection efficiency and thus was not utilized further for these studies. The Jurkat cells were transiently transfected using the electroporation protocol using the Neon Transfection System described in the methods section of this paper. Electroporation resulted in a lower death rate and ~33% transfection efficiency.

To use the FRET-sensor to define Zn^{2+} in Jurkat cells, a calibration protocol had to be developed. A standard calibration protocol performed on HeLa cells (Figure 5, Panel A) could not be used because the Jurkat cells are suspension cells and would be washed away with any attempt to wash out the TPA used to achieve R_{min}. A modified version of the standard protocol was attempted using Jurkat cells transiently transfected with ZapCV2 and divided into three wells, with one well measured as resting, one well treated with TPA for R_{min}, and one well treated with Zn^{2+} for R_{max}. The data was not usable because excessive variability in FRET ratios prevented measurement of stable signals. Thus, this method did not represent a practical method of calibration. We decided to reverse the order of TPA and Zn^{2+} treatments in the calibration protocol to eliminate the need for the TPA washing step. The optimized protocol was as follows. First, the

resting sensor signal was measured. Then, a Zn^{2+} solution containing 1 uM Zn^{2+}, 0.5 uM pyrathione, and 0.001% saponin was added to achieve R_{max}. Then a saturating amount of TPA (50 uM) was added to achieve R_{min}. Several trials revealed that adding 1 uM Zn^{2+} produced a more stable R_{max} than 10 uM Zn^{2+}, which produced FRET ratios that were too unstable to analyze. This optimized protocol produced a stable enough R_{max} and R_{min} for successful analysis (Figure 5, Panel B).

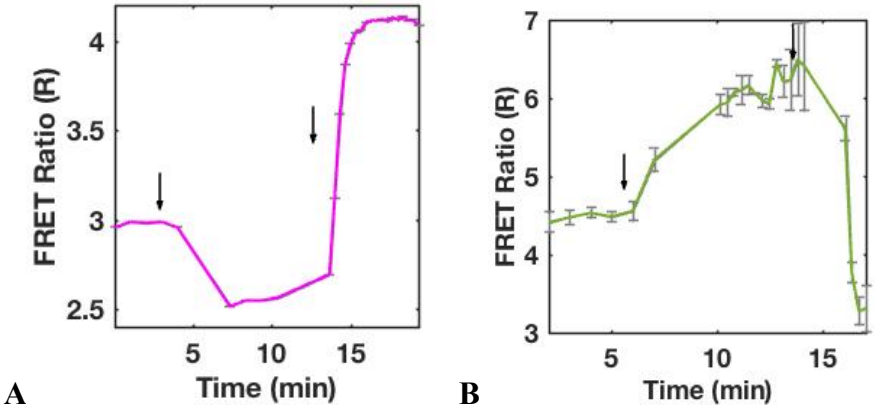

Figure 5: Optimization of calibration of Jurkat cells.
Panel A. A standard calibration of HeLa cells expressing NES-ZapCV2. At the first arrow 20 uM TPA is added to chelate Zn^{2+}*. At the second arrow cells are washed three times with imaging buffer, followed by addition of 200 nM buffered* Zn^{2+} *and 0.5 uM pyrithione. (Data courtesy of Molly Carpenter.) Panel B. Optimized calibration of Jurkat cells expressing NES-ZapCV2. At the first arrow 1 uM* Zn^{2+}*, 0.001% saponin, and 0.5 uM pyrithione. At the second arrow instead of washing, cells are flooded with 50 uM TPA. Data in panel B represents the mean +/- s.e.m. of the FRET ratio from 5 cells.*

Once transfection and sensor calibrations were optimized, we worked to express both the sensor and other genetic tools, such as templates for shRNA expression. Although the cells did not tolerate transient transfection of the two tools well, the creation of a cell line stably expressing the Zn^{2+} sensor allowed for further manipulation of the cells. Cells that were transiently transfected with both NES-ZapCV2 and MTF1 shRNA

with an mCherry reporter (Figure 6, Panels A and B) display cell shape irregularity. This irregularity could be an indication of poor cell health, resulting in low dynamic range Zn^{2+} calibrations (Figure 7, Panel B). In comparison, a larger number of cells in the population of stable NES-ZapCV2 sensor-expressing cells (Figure 6, Panels C and D) have a more uniformly round shape. More cells are also able to be monitored in any given field of view when all cells are expressing the sensor, allowing larger sample size for data analysis (Figure 7, Panels C and D). However, the stable NES-ZapCV2 Jurkat cell line displayed dimming of sensor signal after approximately 2-3 weeks of growing after freezing. The reliable window for usable cells from this stable cell line was about 1-2 weeks.

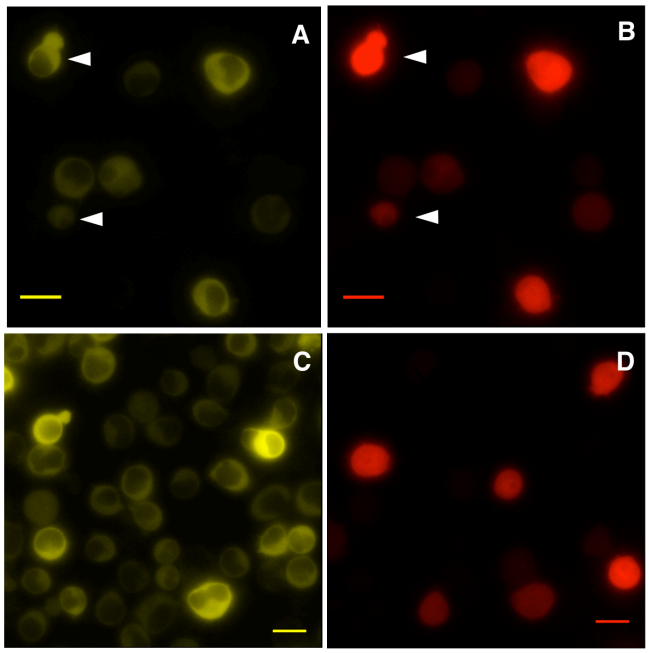

Figure 6: Expression of two orthogonal tools in Jurkat cells.
Arrows indicate abnormal cells. Scale bar = 50um. Panel A. FRET channel image of Jurkat cells transiently transfected by electroporation with NES-ZapCV2 and MTF1 shRNA. Panel B. mCherry channel image of Jurkat cells transiently transfected by electroporation with NES-ZapCV2 and MTF1 shRNA. Panel C. FRET channel image of stable NES-ZapCV2 Jurkat cells transiently transfected by electroporation with MTF1 shRNA. Panel D. mCherry channel image of stable NES-ZapCV2 Jurkat cells transiently transfected by electroporation with MTF1 shRNA.

b. MTF1 knockdown effect on cytosolic Zn^{2+} in Jurkats

If MTF1 knockdown prevents the cell from detecting conditions of excess Zn^{2+} and thus from acting to maintain homeostasis, we hypothesized Jurkats with MTF1 knocked down via shRNA might display different concentrations of labile Zn^{2+} in the cytosol.

The sensor is 49% saturated in the cytosol of cells expressing scrambled control shRNA (Figure 7, Panel A). This agrees with the fractional saturation of wild type Jurkats expressing NES-ZapCV2. The sensor appeared to be more saturated (82%) in Jurkats that were transiently transfected with both tools (Figure 7, Panel B). However, once conditions were optimized so the dynamic range was comparable, the sensor was 53% saturated; about equivalently saturated in cells expressing both scrambled control and MTF1 shRNA (Figure 7, panel C and Table 1). These results suggest that knocking down MTF1 in Jurkat cells doesn't significantly alter the resting zinc concentration in the cytosol. However, one caveat of this conclusion is that we don't know the extent of MTF1 knockdown in the stable cells.

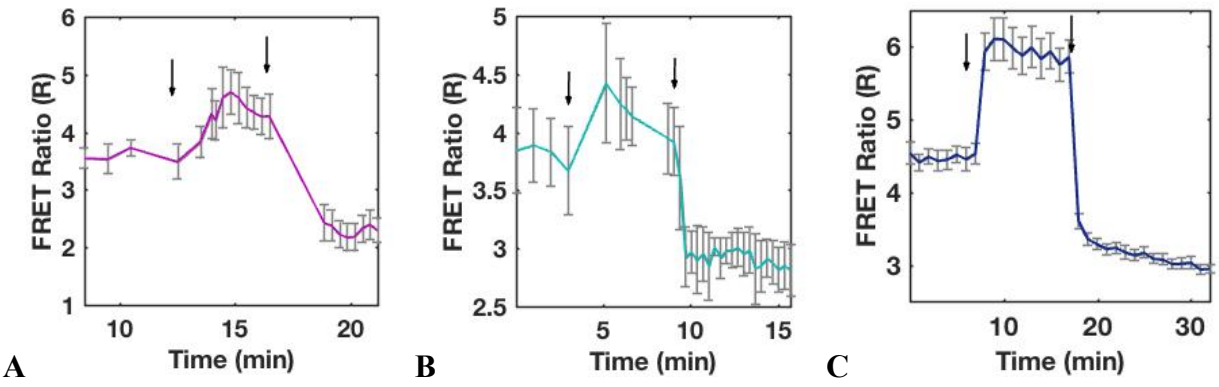

Figure 7: Calibration of cells expressing MTF1 shRNA.
First arrow indicates addition of Zn^{2+}*, second arrow indicates addition of chelator. Panel A. Calibration of stable NES-ZapCV2 Jurkat cells transiently expressing scrambled control shRNA. Data represents the mean +/- s.e.m. of the FRET ratio from 6 cells. Panel B. Calibration of wild type Jurkat cells transiently transfected and expressing both NES-ZapCV2 and MTF1 shRNA, low dynamic range. Data represents the mean +/- s.e.m. of the FRET ratio from 4 cells. Panel C. Calibration of stable NES-ZapCV2 Jurkat cells expressing MTF1, high dynamic range. Data represents the mean +/- s.e.m. of the FRET ratio from 4 cells.*

	Scrambled control (SC)	**MTF1 shRNA (transient sensor expression)**	**MTF1 shRNA (stable expression sensor)**
Dynamic range	1.92	1.54	1.94
Fractional saturation	49%	82%	53%
Free Zn^{2+}	1.94 nM	27.43 nM	2.45 nM

Table 1: Scramble control vs MTF1 shRNA expression and Zn^{2+} concentration
Data represents the average from cells described in Figure 7.

c. Jurkat proliferation under different Zn^{2+} growth conditions

A proliferation assay was performed to determine the optimal and lethal concentrations of Zn^{2+} in media for Jurkat growth. On day 1, each well contained the number of cells plated ($1x10^5$ cells/mL) except the well with 200 uM Zn^{2+} added, which contained $1x10^4$ cells. The extremely high amount of extracellular Zn^{2+} likely caused immediate stress to the cells, killing many in a short amount of time. A large amount of a metal in the media is toxic to cells. Subsequent proliferation of these cells in the highest Zn^{2+} conditions was notably stunted, reaching a final density of $1x10^5$ cells/well after 4 days of growth. Optimal cell proliferation was achieved in the 20 uM Zn^{2+} condition, reaching a final density of 2.25×10^6 cells/well (Figure 8).

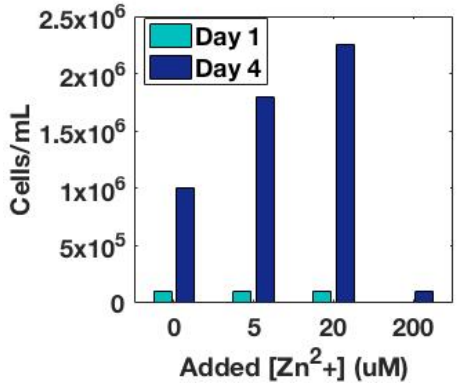

Figure 8: Proliferation of Jurkats under different Zn^{2+} conditions.
Cells were counted by hemocytometer following the protocol described in the methods section of this paper. The wild type Jurkat cells were plated in duplicate for each condition at a starting concentration of $1x10^5$ cells/well and counted at days 1 and 4. Data obtained in collaboration with Molly Carpenter.

d. Free Zn^{2+} in the cytosol under different Zn^{2+} growth conditions

Given the importance of Zn^{2+} in the functioning of the immune system and its involvement in the intracellular signaling pathway of T cells during activation, we wanted to investigate the effect of growth in different concentrations of Zn^{2+} on free cytosolic Zn^{2+} levels in the Jurkat cells. Stable NES-ZapCV2 Jurkat cells were plated at a density of $1x10^5$ cells/well in 0, 20, and 50 uM added Zn^{2+} media for 24 hours and 4 days. The concentrations of Zn^{2+} were selected based on results of the proliferation assay described above, with 20 uM as the ideal condition for maximum proliferation and the 50 uM condition as a high Zn^{2+} state intended to stress the cells without excessive and immediate cell death. Imaging was carried out with the wide field fluorescence microscope using the settings described in the methods section of this paper.

After 24 hours, data was obtained for all three Zn^{2+} growth conditions (Figure 9, Table 2). The dynamic range of the sensor was 2.73, 2.35, and 3.15 for the 0 uM, 20 uM, and 50 uM Zn^{2+} conditions, respectively. The high dynamic range and similarity among the three trials suggests that the concentration of Zn^{2+} calculated from the fractional saturation will be more accurate and not overestimated. The fractional saturation of the sensor was comparable between the 0 uM and 20 uM conditions, at 58% and 53% respectively. The calculated concentrations of free Zn^{2+} for these two conditions were 4.14 and 2.51 nM, suggesting that the amount of free Zn^{2+} does not vary largely between the 0 and 20 uM conditions after 24 hours. The fractional saturation of the 50 uM Zn^{2+} condition was higher than that of the 0 and 20 uM conditions at 72%. The calculated concentration of free Zn^{2+} in the cytosol was 16.33 nM; over three times higher than that of the 0 or 20 uM condition after 24 hours.

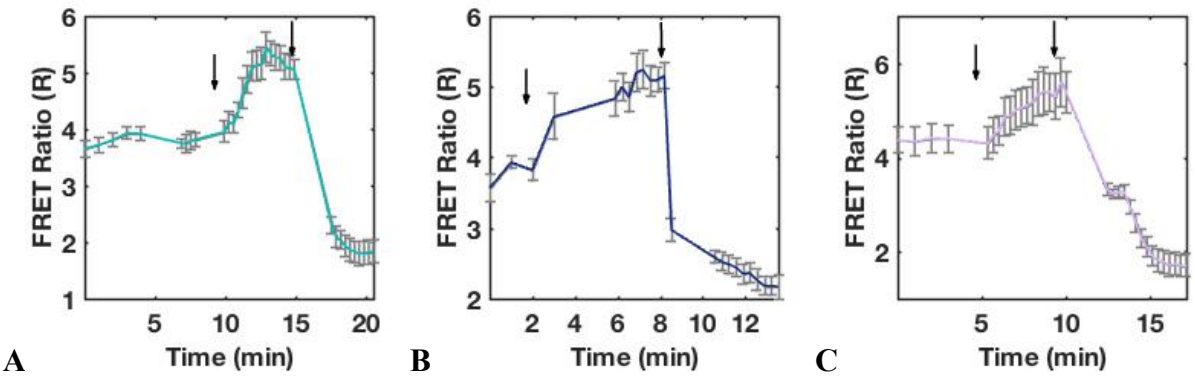

Figure 9: Calibration of NES-ZapCV2 in Jurkat cells grown in different Zn^{2+} conditions for 24 hours. *The first arrow indicated the addition of* Zn^{2+}*, the second arrow indicated the addition of chelator. All cells used were stable NES-ZapCV Jurkat cells. Panel A. 0 uM added* Zn^{2+}*. Data represents the mean +/- s.e.m. of the FRET ratio from 5 cells. Panel B. 20 uM added* Zn^{2+}*. Data represents the mean +/- s.e.m. of the FRET ratio from 6 cells. Panel C. 50 uM added* Zn^{2+}*. Data represents the mean +/- s.e.m. of the FRET ratio from 5 cells.*

After 4 days, the cells in the 0 uM added Zn^{2+} were unhealthy and hard to image, so only cells grown in the 20 and 50 uM Zn^{2+} conditions were calibrated (Figure 10, Table 2). The differences in cytosolic free Zn^{2+} between the two conditions are even more pronounced after 4 days than after 24 hours: 4.97nM in the 20 uM condition and 225.05 nM in the 50 uM condition. The fractional saturations of the sensor were 67.54% and 92.61% for the 20 and 50 uM conditions, respectively. However, the dynamic range for the sensor was 2.24 in the 20 uM condition and 1.71 in the 50 uM condition. The lower dynamic range for the higher Zn^{2+} condition is likely an indication of the stressed state of the cells and poorer cell health, which can impact the ability of the sensor to accurately indicate the concentration of Zn^{2+}.

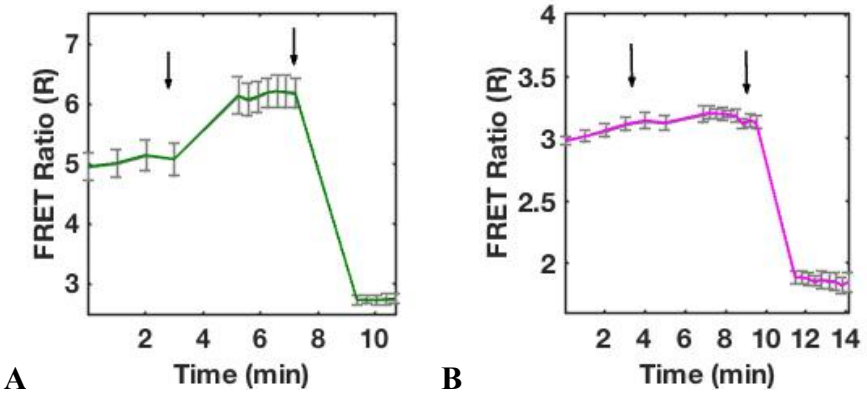

Figure 10: Calibration of NES-ZapCV2 in Jurkat cells grown in different Zn^{2+} conditions for 4 days. *The first arrow indicated the addition of* Zn^{2+}*, the second arrow indicated the addition of chelator. All cells used were stable NES-ZapCV2 Jurkat cells. Panel A. 20 uM added* Zn^{2+}*. Data represents the mean +/- s.e.m. of the FRET ratio from 6 cells. Panel B. 50 uM added* Zn^{2+}*. Data represents the mean +/- s.e.m. of the FRET ratio from 5 cells.*

[Zn^{2+}] added	Time in growth conditions	Dynamic range	Fractional saturation	Free Zn^{2+} in cytosol (nM)
0uM	24 hrs	2.73	58%	4
	4 days	x	x	x
20uM	24 hrs	2.35	53%	2
	4 days	2.24	67%	4
50uM	24 hrs	3.15	72%	16
	4 days	1.71	92%	225

Table 2: Summary of sensor calibration data in Jurkat cells grown in different Zn^{2+} conditions.

e. IL-2 ELISA time course

Since the key characteristic of T cells is their unique ability to be stimulated in order to coordinate the adaptive immune response, we wanted to use our sensor as a tool to study Zn^{2+} in conditions of T cell stimulation. First, we had to confirm that the Jurkats were actually being stimulated and producing IL-2 to ensure that the Jurkat cells could

serve as a model of T cell behavior. A time course was performed in order to confirm stimulation of the stable NES-ZapCV2 Jurkat cells with the Dynabeads. Supernatant samples were collected from separate wells of stimulated cells at 0, 2, 4, 6, 22, 24, and 96 hours post-stimulation. An ELISA was performed to measure concentration of IL-2, the key cytokine produced by T cells upon stimulation. A standard curve was generated for analysis of results by preparing standards with known IL-2 concentrations of 1500, 600, 240, 96, 38.4, 15.36, and 0 pg/mL. The concentrations of the samples collected from the time course stimulation of the Jurkat cells with the Dynabeads was determined using the measured absorbance and the equation from the standard curve. Anti-CD3 and CD28 antibodies on the surface of the Dynabeads bind the T-cell receptor and CD28 costimulatory molecule on the surface of the T cell in order to initiate the process of stimulation. The concentrations of IL-2 in the samples collected 0 and 2 hours post-stimulation were 2.84 and 2.25 pg/mL respectively. This indicates that two hours after stimulation, the Jurkats had not yet produced and secreted an appreciable amount of IL-2. This is consistent with the process of stimulation with antibodies, because the extracellular binding of antibody initiates a signaling cascade intracellularly. This cascade eventually activates transcription factors, which then initiate transcription of IL-2 that is subsequently translated into the protein product for secretion. The cell processes of transcription and translation are not immediate and take time to carry out. These results indicate that the process to produce IL-2 may take longer than 2 hours for a detectable difference in IL-2 secretion. However, after 4 hours the Jurkats displayed successful stimulation with an IL-2 concentration of 15.44 pg/mL. The IL-2 concentration continued to increase after 6 hours to 23.41 pg/mL, but after 22 hours the concentration was very

similar at 23.50 pg/mL. This could be due to differences in individual cell population between these two wells, and sufficient wells should be plated to allow samples to be pulled at each time point in duplicate or triplicate to account for or identify such differences. 24 hours post-stimulation, the IL-2 concentration reached 34.94 pg/mL.

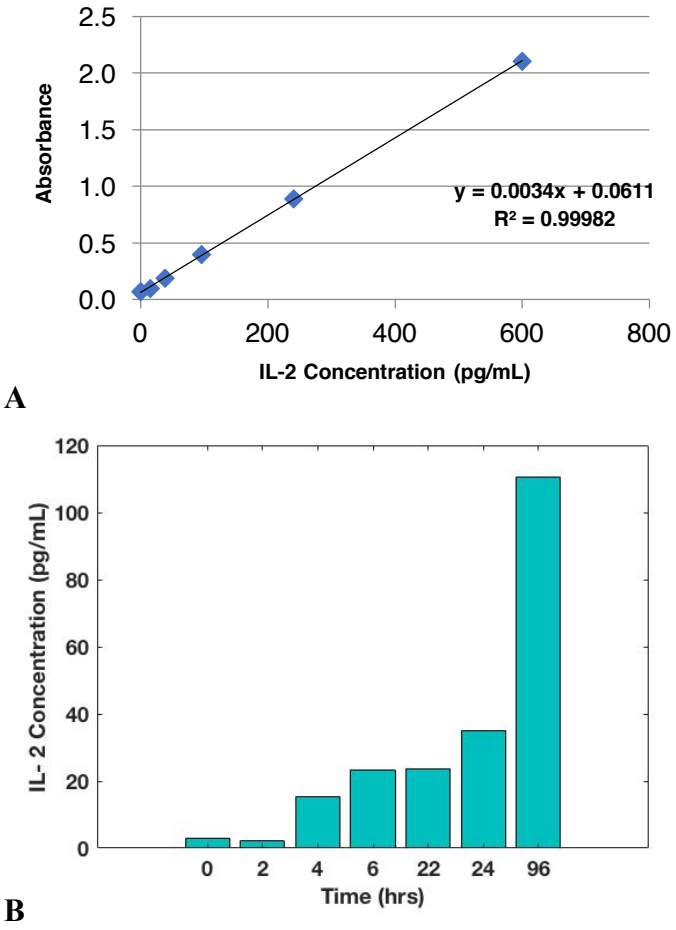

Figure 11: Stimulation of NES-ZapCV2 stable Jurkat line. *Panel A. standard curve to confirm linearity of ELISA for IL-2 detection. Panel B. IL-2 production of stimulated Jurkat cells over 4 days.*

f. IL-2 ELISA for dynabead/cell number titration

Although we could stimulate the Jurkats under the conditions outlined by the manufacturer the concentration of IL-2 produced was low. We decided to test for the optimum concentration of cells to stimulate as well as the optimum ratio of Dynabeads:cells. We wanted to determine whether an adequate number of cells were being stimulated and whether an adequate amount of Dynabeads were being used to stimulate the cells. This trial utilized wild type Jurkat cells rather than the stable NES-ZapCV2 Jurkats because of issues with low proliferation and sensor expression in the stable cell line. The cell densities plated were the recommended cell density per manufacturer's instructions of $8x10^4$ cells/well as well as two higher concentrations: $1.6x10^5$ cells/well and $3.2x10^5$ cells/well. Each of these concentrations were then stimulated with Dynabeads at a ratio of beads:cells of 1:1 (recommended by manufacturer), 3:1, and 10:1. Additionally, two unstimulated wells were included for the highest and lowest concentration of cells. The cells were incubated after stimulation, and supernatant samples were pulled 24 hours post-stimulation for an IL-2 ELISA. Interestingly, the stimulation with parameters following the manufacturer's protocol for both cell density and bead:cell ratio resulted in an IL-2 concentration of 202.44 pg/mL. This is over four times as high as the IL-2 concentration of the stable NES-ZapCV2 Jurkats 24hrs post stimulation with manufacturer's parameters. The stable NES-ZapCV2 Jurkats are producing the sensor, which may occupy cell machinery and resources for protein production and account for the lower amount of IL-2 produced and secreted. The results shown were as expected: as either cell density or bead:cell ratio was increased, IL-2 production increased. A higher cell density of $1.6x10^5$ cells/well with a 3:1 ratio of cells

to beads resulted in an IL-2 concentration of 1271.48, and should be the parameters selected to ensure adequate stimulation for detection with an IL-2 ELISA. (Table 3)

Number of cells	Ratio of Dynabeads:cells	Absorbance (at 450-550)	Calculated concentration (pg/mL)
$8x10^4$ cells/well	0:1 (unstimulated)	0.0388	-15
	1:1	0.6275	202
	3:1	1.8438	652
	10:1	3.6051	1305
$1.6x10^5$ cells/well	1:1	1.7823	630
	3:1	3.5139	1271
	10:1	High signal	--
$3.2x10^5$ cells/well	0:1 (unstimulated)	0.0522	-10
	1:1	1.7993	636
	3:1	High signal	--
	10:1	High signal	--

Table 3: Optimization of stimulation conditions of Jurkat cells.

VI. Discussion:

Our Zn^{2+} sensors allow us a glimpse of the biology of Zn^{2+} within the cell. In this work, our focus was on the application of these tools to Jurkat T cells to elucidate the behavior of Zn^{2+} in immune cells. Jurkat cells were a novel cell type for the lab, so we began with the optimization of protocols to successfully use the Zn^{2+} sensors. Our results show the importance of testing - and modifying if necessary - cell growth conditions, transfection methodology, and imaging protocols to successfully utilize Zn^{2+} sensors in a novel cell type. Using NES-ZapCV2 as a reporter, I tested the effect of manipulation of a native Zn^{2+} sensor and of changes in available Zn^{2+} to the cytosolic Zn^{2+} concentration in immune cells. I also found that expression of the sensor may alter the ability of Jurkat cells to activate. These experiments lay the groundwork for applying tools reliably able to parse out the role of Zn^{2+} in the activation of T cells.

In order to appropriately apply FRET sensors to investigate Zn^{2+} biology, it is necessary to optimize conditions to ensure the sensors are functioning properly with high dynamic range.[15] The results in this work support this conclusion; this is highlighted in the experiments performed with the MTF1 shRNA and when Zn^{2+} growth conditions were altered. When cells were transiently transfected with both the sensor and the MTF1 shRNA, the dynamic range was 1.54 (see Table 1). This is much lower than the dynamic range when cells stably expressing the Zn^{2+} sensor were only singly transfected with shRNA (dynamic range of 2 or higher). We hypothesize that the double transfection induced additional stress on the cells, making them less healthy than the cells that were only singly transfected. An unhealthy state was also observed in cells grown in very high Zn^{2+} conditions prior to

imaging; cells grown in 80 uM Zn^{2+} for 4 days were too unhealthy to perform reliable calibration experiments.

Using optimal calibration conditions our findings illuminated key features of Jurkat cells that differ from other cell types previously studied with Zn^{2+} sensors. A high concentration of cytosolic free Zn^{2+} was observed consistently throughout our experiments, which supports the potential of Zn^{2+} as a signaling species in the pathway of an immune response because of its increased availability. Growth in different Zn^{2+} conditions altered the cytosolic concentration of Zn^{2+}, with increased levels of Zn^{2+} in the cells grown in media with higher concentrations of added Zn^{2+}. The cells grown in Zn^{2+} conditions for 4 days showed a greater difference in cytosolic Zn^{2+} concentration between the 20 and 50 uM added Zn^{2+} conditions compared to the cells grown in the Zn^{2+} conditions for 24 hours. This suggests that extended periods of time in high Zn^{2+} conditions lead to accumulation of Zn^{2+} in the cytosol over a period of days, which could have potential implications for studying states of chronic Zn^{2+} disturbance in high or low amounts. Little is known about the relative expression of Zn^{2+} transporters and buffers in Jurkat cells as compared to other cell lines. In the future, it would be interesting to better understand if differences in protein expression that confer this high resting Zn^{2+} concentration in the cytosol.

Because cytosolic Zn^{2+} is higher in Jurkat cells than in adherent cells studied in the lab, we hypothesized that knocking down MTF1, a protein involved in coordinating the cellular response to Zn^{2+}, might alter cytosolic Zn^{2+}. After knocking down MTF1 with shRNA, no difference in cytosolic Zn^{2+} concentration was shown when compared to the trial transfected with scrambled control shRNA. These results support the highly redundant model of Zn^{2+} homeostasis and resulting tight regulation. They suggest that multiple different proteins are

key players in coordinating the cell's response to Zn^{2+}, and that others can compensate when one is removed. It must be noted that knocking down expression with shRNA should be confirmed with a Western blot to ensure decreased production of the protein being targeted. In future studies, a Western blot for MTF1 should be performed to confirm that the lack of change in cytosolic Zn^{2+} concentration is indeed despite the absence of MTF1.

The creation of the stable NES-ZapCV2 Jurkat cell line was important for solving the problem with dynamic range, but other challenges must be considered when working with this stable cell line. First, the brightness of both FPs diminished over time; after approximately 3 weeks, the sensor was no longer bright enough to successfully image. Dimming of a stably expressed sensor over time has been observed in MCF10A human mammary cell lines as well, but it is unknown why the sensor dims over time in a stable cell line. To solve this problem, cells from the stable cell line were unfrozen from cryopreservation stocks and only used for 2-3 weeks in experiments. The second consideration that must be made when using the stable cell line is the impact of constitutive sensor expression on the other activities of the cell. We hypothesize that the constitutive production of a sensor by a cell requires a large amount of cell resources and put a strain on cell machinery. This could decrease the ability of the cell to produce other products. Our results comparing the IL-2 production of the stable NES-ZapCV2 Jurkat cell line and the wild type Jurkats support this hypothesis: 24 hours after stimulation with identical parameters, the stable cell line IL-2 concentration was 34.94 pg/mL while the wild type was 652.93 pg/mL. Therefore, if IL-2 production is used as a measure of degree of stimulation, results should only be compared between trials performed on cells of the same cell line.

Although progress was made in optimizing the parameters for Jurkat stimulation and subsequent detection of IL-2 via ELISA, the protocol has yet to be successfully applied to Jurkats in different Zn^{2+} conditions. The tools developed in this thesis have paved the way to studying Jurkat stimulation and Zn^{2+} by establishing Jurkat cells as a model system. Here we first demonstrated an ability to monitor and image Zn^{2+} with genetically encoded FRET sensors and manipulation of Zn^{2+} growth conditions. By using the Jurkat cell line stably expressing ZapCV2, we have also unlocked the potential to express orthogonal tools to investigate perturbations in Zn^{2+} homeostasis proteins. With access to shRNA for all Zn^{2+} transporters and metallothioneins, we have the potential to knock down expression of many key players in the cell's system of Zn^{2+} regulation and monitor cytosolic Zn^{2+} concentration. Additionally, we confirmed Jurkat cells as a model of normal T cell behavior by measuring stimulation. With the protocols developed in this thesis, we hope to continue investigations by combining stimulation with varying Zn^{2+} growth conditions. The aims of this investigation are two-fold. First, Jurkat cells grown in different Zn^{2+} conditions will be stimulated and IL-2 production measured with an ELISA in order to see if IL-2 production varies depending on Zn^{2+} growth condition. Second, it would also be interesting to perform a long-term imaging experiment of the sensor in Jurkat cells to monitor cytosolic Zn^{2+} upon stimulation. By using the tools and protocols developed in this thesis, we hope to further tease out the role of Zn^{2+} in T cell immune function.

VII. Acknowledgements

First, I would like to thank Dr. Amy Palmer from the bottom of my heart for the opportunity to conduct research in her lab and for her continuous support and encouragement. You have had a profound influence in fostering my love of research. Thank you for challenging and inspiring me throughout my time in the lab.

I would also especially like to thank Molly Carpenter for being an exceptional mentor in every possible way. She has given me guidance and direction both for my work in the lab and my life outside the lab, and I am so grateful for her expertise and advice. Thank you for the immense amount of support and countless hours you have spent mentoring me in the lab.

Additionally, I am grateful to Dave Simpson for helping me seamlessly adjust to working in the lab and for his helpful feedback and endless patience. Thank you for all you have done to make me feel welcome and supported in the lab.

The work in this thesis was only possible through incredible support from the members of the Palmer lab: Kyle, Lara, Maria, Esther, Lynn, Ali, Dilara, Kelsie, Mike, Erin, Natalie, and Grant. I cannot express what a wonderful experience it has been working with you in such a collaborative and positive environment. I am so appreciative to you all for your help and input along this process.

VIII. References

1. Prasad, A. S. Discovery of human zinc deficiency: 50 years later. *J. Trace Elem. Med. Biol.* **26,** 66–69 (2012).
2. Ibs, K.-H., Function, Z. I. & Rink, L. Immunity Enhanced by Trace Elements. *Sci. York* **133,** 1452S–6S (2003).
3. Hirano, T. *et al.* Roles of Zinc and Zinc Signaling in Immunity: Zinc as an Intracellular Signaling Molecule. *Advances in Immunology* **97,** 149–176 (2008).
4. Chaplin, D. D. Overview of the immune response. *J. Allergy Clin. Immunol.* **125,** (2010).
5. Bonilla, F. A. & Oettgen, H. C. Adaptive immunity. *J. Allergy Clin. Immunol.* **125,** (2010).
6. Kaltenberg, J. *et al.* Zinc signals promote IL-2-dependent proliferation of T cells. *Eur. J. Immunol.* **40,** 1496–1503 (2010).
7. Eide, D. J. Zinc transporters and the cellular trafficking of zinc. *Biochimica et Biophysica Acta - Molecular Cell Research* **1763,** 711–722 (2006).
8. Thambiayya, K., Kaynar, A. M., St Croix, C. M. & Pitt, B. R. Functional role of intracellular labile zinc in pulmonary endothelium. *Pulm. Circ.* **2,** 443–451 (2012).
9. Paski, S. C. & Xu, Z. Labile intracellular zinc is associated with 3T3 cell growth. *J. Nutr. Biochem.* **12,** 655–661 (2001).
10. Holland, T. C., Killilea, D. W., Shenvi, S. V. & King, J. C. Acute changes in cellular zinc alters zinc uptake rates prior to zinc transporter gene expression in Jurkat cells. *BioMetals* **28,** 987–996 (2015).
11. Babula, P. *et al.* Mammalian metallothioneins: properties and functions. *Metallomics* **4,** 739–750 (2012).
12. Bozym, R. A. *et al.* Free zinc ions outside a narrow concentration range are toxic to a variety of cells in vitro. *Exp. Biol. Med. (Maywood).* **235,** 741–50 (2010).
13. Hardyman, J. E. J. *et al.* Zinc sensing by metal-responsive transcription factor 1 (MTF1) controls metallothionein and ZnT1 expression to buffer the sensitivity of the transcriptome response to zinc. *Metallomics* **8,** 337–343 (2016).
14. Qin, Y. *et al.* Direct comparison of a genetically encoded sensor and small molecule indicator: Implications for quantification of cytosolic Zn2+. *ACS Chem. Biol.* **8,** 2366–2371 (2013).
15. Carpenter, M. C., Lo, M. N. & Palmer, A. E. Techniques for measuring cellular zinc *. **611,** 20–29 (2016).
16. Qin, Y., Dittmer, P. J., Park, J. G., Jansen, K. B. & Palmer, A. E. Measuring steady-state and dynamic endoplasmic reticulum and Golgi Zn2+ with genetically encoded sensors. *Proc. Natl. Acad. Sci. U. S. A.* **108,** 7351–6 (2011).
17. Dingwall, C. & Laskey, R. A. Nuclear targeting sequences--a consensus? *Trends Biochem. Sci.* **16,** 478–81 (1991).
18. Rekas, A., Alattia, J. R., Nagai, T., Miyawaki, A. & Ikura, M. Crystal structure of venus, a yellow fluorescent protein with improved maturation and reduced environmental sensitivity. *J. Biol. Chem.* **277,** 50573–50578 (2002).
19. Abraham, R. T. & Weiss, A. Jurkat T cells and development of the T-cell receptor signalling paradigm. *Nat. Rev. Immunol.* **4,** 301–8 (2004).